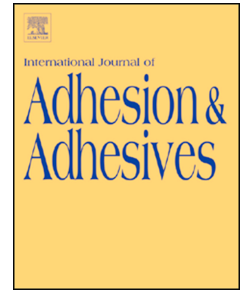


Journal Pre-proof

Fracture mechanisms of hybrid adhesive bonded joints: effects of the stiffness of constituents

Armin Yousefi Kanani, Yiding Liu, Darren J. Hughes, Jianqiao Ye, Xiaonan Hou



PII: S0143-7496(20)30112-3

DOI: <https://doi.org/10.1016/j.ijadhadh.2020.102649>

Reference: JAAD 102649

To appear in: *International Journal of Adhesion and Adhesives*

Received Date: 28 April 2020

Accepted Date: 12 May 2020

Please cite this article as: Kanani AY, Liu Y, Hughes DJ, Ye J, Hou X, Fracture mechanisms of hybrid adhesive bonded joints: effects of the stiffness of constituents, *International Journal of Adhesion and Adhesives*, <https://doi.org/10.1016/j.ijadhadh.2020.102649>.

This is a PDF file of an article that has undergone enhancements after acceptance, such as the addition of a cover page and metadata, and formatting for readability, but it is not yet the definitive version of record. This version will undergo additional copyediting, typesetting and review before it is published in its final form, but we are providing this version to give early visibility of the article. Please note that, during the production process, errors may be discovered which could affect the content, and all legal disclaimers that apply to the journal pertain.

© 2020 Elsevier Ltd. All rights reserved.

Fracture mechanisms of hybrid adhesive bonded joints: effects of the stiffness of constituents

Armin Yousefi Kanani^a, Yiding Liu^b, Darren J. Hughes^b, Jianqiao Ye^a, Xiaonan Hou^{a,*}

^a Department of Engineering, Engineering Building, Lancaster University, Lancaster, LA1 4YW, UK

^b WMG, University of Warwick, Coventry, CV4 7AL, UK

*Corresponding author's email address: x.hou2@lancaster.ac.uk

Abstract

In this study, different single-lap hybrid joints are used to analyse the effects of the stiffness of the adherends and the adhesive on the failure mechanism. The hybrid joints include a combination of (a) different adherends: aluminium (6082 T6) and PolyPhtalamide (PPA) reinforced with 50% of glass fibre (grade HTV-5H1 from Grivory) and (b) different adhesives: epoxy-based adhesive (Loctite EA 9497) and silane-modified polymer-based adhesive (Teroson MS 9399). Six different single-lap joints are fabricated and analysed. The cohesive parameters of different adhesives against different adherends are determined respectively using single-mode coupons and validated with finite element modelling. Single-lap shear tests are conducted to understand different fracture mechanisms of the joints. Finite element (FE) models using the Cohesive Zone Method (CZM) are developed to simulate the failure of the joints and validated by the testing results. Different failure processes obtained from different hybrid joints combinations are discussed further by analysing the stress distributions along the interfaces of the joints. Finally, the relationship between the stiffness of the constituents of a hybrid adhesive joint and its failure mechanism is summarised. The load vs displacement behaviour of the single-lap joints demonstrate that the stiffness of adherends affects the maximum failure load of the joints with rigid adhesive (epoxy). However, the joint with flexible adhesive (polyurethane) is not sensitive to the stiffness of the adherends. In addition, higher shear stress distribution occurs in the interface adjacent to the adherend with lower stiffness, leading to the failure initiation at the PPA side regardless of adhesive types.

Keywords: hybrid joint; joint stiffness; adherends; adhesives; cohesive zone model; finite element modelling

1. Introduction

With the rapid development of new engineering materials, multi-material structures are now widely used to achieve the desired performance. Consequently, the use of adhesive joining techniques is increasing due to their advantages over traditional joints, such as easy manufacturing, more uniform stress distribution, and the possibility of joining dissimilar adherends. However, there are still some barriers in using adhesive joining techniques in practice due to a lack of an accepted theory, which describes the fracture mechanism of the hybrid joints and summarises the factors affecting the performance of the joints. As the hybrid joint involves the combination of two different adherends with different mechanical properties, leading to a more complicated fracture mechanism in practice, for instance, mixed-mode failure (crack may be initiated from the interface and grow into the adhesive layer, or vice versa).

In recent years, several experimental works have been conducted that explore the factors affecting the strength of adhesive joints, such as the type of adhesives, the materials of adherends and the joint configurations (overlap length, adherend and adhesive thickness). Wu et al. [1] corrected Goland and Reissner's solution by modifying their classical equation for analysing the adhesive layer in dissimilar adherends with different thicknesses and lengths. Sawa et al. [2] analysed the single-lap joint of dissimilar adherends (aluminium bonded to mild steel) under a tensile shear loading. Their results show that the stress singularity increases at the free edges of the interface with lower stiffness, and the thinner adherend. Pinto et al. [3] evaluated the tensile strength of single-lap joints with different adherends (polypropylene (PP), polyethylene (PE), carbon-epoxy, and glass-polyester composites). They found that increasing the adherends' stiffness reduces the joint bending and diminishes stress at the overlap edges and, consequently, increases the joint strength. Reis et al. [4] studied the influence of the adherend's stiffness on the shear strength of the single-lap adhesive joint by using three different adherends (laminated composite, high elastic limit steel, and the 6082-T6 aluminium alloy). Their studies concluded that the effects of the overlap length on the shear strength depend on the stiffness of the adherends. Pereira et al. [5] showed that the increase in the thickness of the adherend decreases the rotation angle of the joint and the peak plastic strain. Da Silva et al. [6] and Nunes et al. [7] studied the influences of the adhesive type (epoxy and ductile adhesives) and thickness of the bond-line on the single-lap joint strength. It can be concluded that the shear strength of SLJ increases by decreasing the adhesive thickness or increasing the adhesive toughness.

Cohesive Zone Modelling (CZM) has been widely used in the simulation as it allows multiple failure paths in the middle of the adhesive or along the interface to predict failure. There are various techniques (direct and indirect methods) to obtain CZM parameters (t_n , G_{IC} , t_s , G_{IIC}) by using double cantilever beam (DCB), end notch flexure (ENF) and single-lap joint (SLJ) tests. Zhu et al. [8] used the direct method (J -integral) to obtain the traction-separation laws of both mode 1 and mode 2 with sandwich specimens for polyurea/steel interfaces. Their results show that the traction values in both

cases depend on the loading rates. An increase in the loading rate increases the cohesive peak stress, while the critical opening displacement decreases. Ruadwska [9] and Alves et al. [10] analysed the tensile strength of the bonded joint between similar and dissimilar material by using an indirect method considering both experimental and CZM approaches for fracture predictions. Katsivalis et al. [11] noted that the validated cohesive parameters depend on several factors, including the bond-line thickness (t_A), the adherends' stiffness and surface chemistry. Wang and Qiao [12] compared shear-mode (model II) fracture toughness of the wood-wood and wood-FRP by using tapered end-notched flexure (TENF) specimens. Their results show that the fracture toughness of the wood-FRP interface is lower than the value of wood-wood bonded interfaces. Tvergaard et al. [13] noted that the interface roughness and crack growth along the bond-line of the dissimilar joints under a mixed-mode loading condition strongly depend on the elastic modulus ratio E_1/E_2 of adherends.

Most of the previous numerical works used a single layer of the cohesive element in the bond-line to simulate the adhesive layer, which is accurate enough for identical adherend joints. Nonetheless, the method cannot describe the failure process for the hybrid joint and estimate the strength of the joint accurately. Since the change of the adherend changes the interaction between adhesive and adherend due to roughness and chemical links [14].

The objectives of this work are to predict joints strength and analyse stress distributions along bond-lines, and to understand the failure mechanisms of the single-lap joints geometry with dissimilar adherends by comparing to the performances of identical single-lap joints. Finite element models were developed to predict the strength of the hybrid joints by considering the effects of their adherend stiffness. Experimental works on the six different kinds of single-lap joints were conducted, which consist of three categories of adherend combinations (AL bonded to AL, polyphthalamide (PPA) bonded to PPA, and AL bonded to PPA) using two kinds of adhesives (Loctite EA 9497 epoxy adhesive and Terson MS 9399 polyurethane adhesive), to understand their failure performances as well as to validate the FE models. The innovation of the FE models is to use two layers of cohesive elements along the different interfaces between the adhesive bulk and the adherends with different cohesive properties measured from single-mode coupons using the relevant adherends, respectively. This method is approved to provide a more concise strength prediction regarding the hybrid joint combinations. Stress distribution analysis, stiffness degradation analysis, as well as failure surface observations, were also carried out to obtain a better understanding of the failure mechanism of the hybrid joints.

2. Mechanical Test

2.1. Material properties of adherends and adhesives

The adherends used in this study were aluminium alloy 6082 T6 (AL) and polyphthalamide (PPA). The PPA material, commercially named Grivory HTV-5H1 black 9205, is a glass fibre (50%) reinforced engineering thermoplastic material based on a semi-crystalline, partially aromatic polyamide. Tensile tests were carried out for both AL and PPA materials based on the ISO EN 485-2:2016 to characterise their mechanical properties, as shown in Table 1. The Young's modulus and elongation at fracture of the AL material were approximately three times and five times higher than the PPA material. This suggests that the AL adherend has higher stiffness and plasticisation allowance before failure compared to the PPA adherend.

Table 1: The bulk property of adherends and adhesives

| Property | AL | PPA | Terson MS 9399 | Loctite EA 9497 |
|----------------------------------|-------------------------|--------------------------|--------------------------|-------------------------|
| Young Modulus (MPa) | 70770 ± 385 | 17620 ± 592 | 3.06 ± 0.21 ^a | 7705.35 ± 468.08 |
| Yield Stress (MPa) | 254.59 ± 3.20 | 241.33 ± 10.4 | 2.56 ± 0.13 | 46.29 ± 3.13 |
| Elongation at fracture (%) | 10.83 ± 0.95 | 1.71 ± 0.04 | 153.03 ± 14.38 | 0.71 ± 0.09 |
| Poisson Ratio | 0.30 ± 0.01 | 0.32 ± 0.04 | 0.44 ± 0.01 | 0.29 ^b |
| Density (tonne/mm ³) | 2.7 × 10 ^{-9b} | 1.65 × 10 ^{-9b} | 1.4 × 10 ^{-9b} | 1.1 × 10 ^{-9b} |

^a Estimated from Neo-Hookean method ^b Manufacturer data

There were two different types of adhesives (Loctite EA 9497 and Terson MS 9399) used in this study. Loctite EA 9497 is a medium viscosity, two-component room temperature curing epoxy, and Terson MS 9399 is a highly viscous, sag-resistance two-component polyurethane adhesive based on silane-modified polymers. Tensile tests were carried out using bulk specimens to obtain the mechanical properties of both adhesives (Table 1), based on ISO 37 (for Terson MS 9399) and ISO527-2 (for Loctite EA 9497). The results show that the modulus of Loctite EA 9497 is about 200 times higher than Terson MS9399 when the samples have the same configuration. In addition, Terson MS 9399 allows significant larger elongation before failure compared to Loctite EA 9497.

2.2. Joint configuration and fabrication

In order to find the cohesive properties: traction (t_n and t_s) and fracture energy (G_{IC} and G_{IIC}) in tensile and shear directions; single-mode coupon tests were carried out, which were double cantilever beam (DCB) and end notched flexure (ENF) tests. Thick adherend shear test (TAST) was specifically used for samples with the polyurethane adhesive and PPA adherends since the failure of the PPA adherends occurs in advance of the failure of the polyurethane adhesive in the ENF tests [15].

As the changes in the adherend materials affect the interaction between adhesives and adherends, resulting in different interface properties; therefore, different bonding families were manufactured to capture the corresponded interface properties. These samples include AL adherends (AL-AL) with

epoxy adhesive; AL adherends (AL-AL) with polyurethane adhesive; PPA adherends (PPA-PPA) with epoxy adhesive and PPA adherends (PPA-PPA) with polyurethane adhesive.

The geometry configurations of the samples for DCB, ENF and TAST tests are shown in Figure 1. DCB test specimens were based on ISO 25217:2009 standard (Figure 1a). The overall length (L_t) for the AL-AL and PPA-PPA specimens were 200 mm and 100 mm, respectively. The initial crack lengths in the AL-AL specimens were $a_0 = 50$ mm and slightly shorter $a_0 = 30$ mm for the PPA-PPA specimens due to the limited length of the PPA plate provided by the manufacturer. The other dimensions such as adherend thickness $t_p = 12$ mm, the adhesive thickness $t_A = 0.56$ mm and width of adherends $B = 25$ mm were the same in both tests, as suggested by ISO 25217:2009 standard.

ENF test specimen was based on ASTM D7905/D7905M, which was adapted to the adhesive joint in this study (Figure 1 b). The overall lengths of the specimens (L_t) were 300 mm and 100 mm for the AL-AL and PPA-PPA samples, respectively. Besides, the magnitudes of other dimensions were the same as the ones in the specimen for the DCB test.

Figure 1c shows the joint configuration for TAST test. The dimensions were as follow: the joint has an artificial crack length of 5 mm in the mid-thickness of the bond-line at one end of overlap, the total length of $L_t = 148$ mm, overlap length of $L_0 = 25$ mm, adherend thickness of $t_p = 12$ mm, the adhesive thickness of $t_A = 3$ mm and the width of adherend equals to $B = 25$ mm.

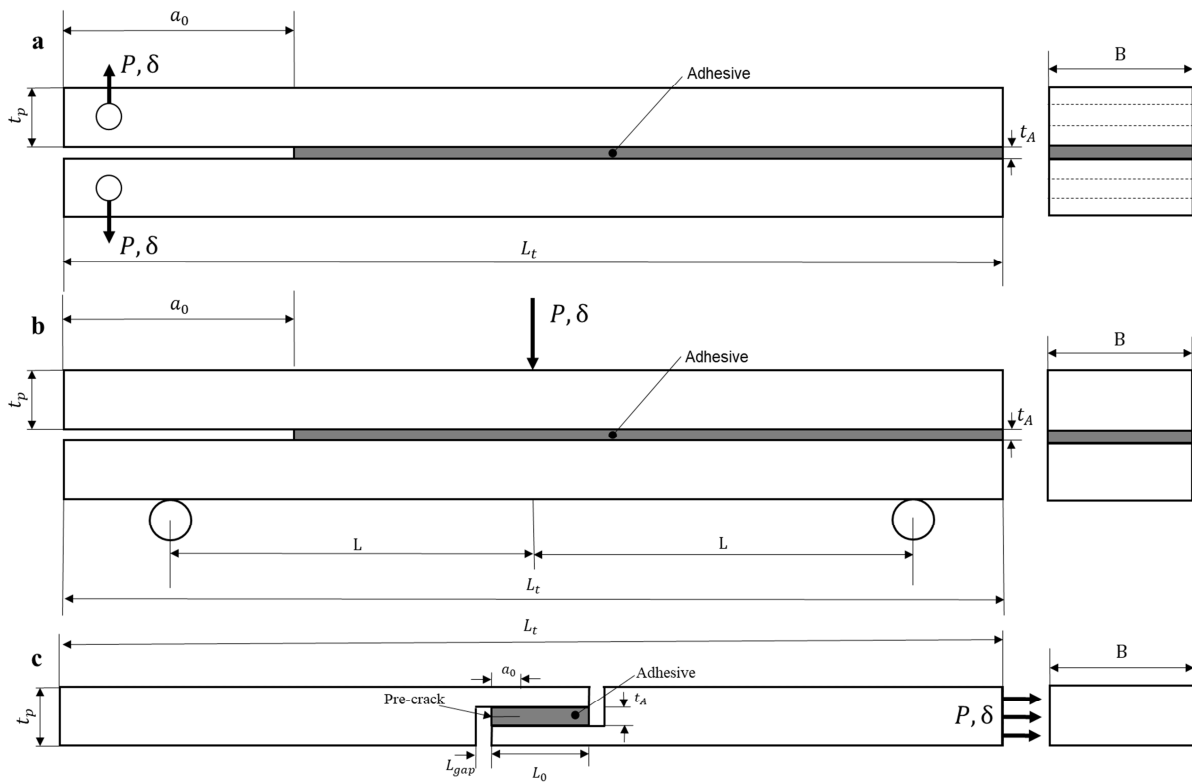


Figure 1: Geometry configurations for samples of (a) DCB (b) ENF (c) TAST tests

Single-lap joints were manufactured with various adherends, which gives three combinations of joints: AL-AL, PPA-PPA, and hybrid joint (AL-PPA), for each adherend combination, two different

adhesives (Loctite EA 9497 and Terson MS 9399) were used. Hence, there were six different single-lap joints in total (Table 2). For the convenience of discussion, the hybrid joint (AL-PPA) was defined as a joint with AL at the top adherend and PPA at the bottom adherend.

Table 2: The combinations of single-lap joint

| ID | Top Adherend | Bottom Adherend | Adhesive |
|---------|--------------|-----------------|-----------------------------------|
| AL-AL | Aluminium | Aluminium | Loctite EA 9497 or Terson MS 9399 |
| AL-PPA | Aluminium | PPA | Loctite EA 9497 or Terson MS 9399 |
| PPA-PPA | PPA | PPA | Loctite EA 9497 or Terson MS 9399 |

The geometry of a single-lap joint had a total length of $L_t = 187.5$ mm and other dimensions were as follow: overlap length of $L_s = 12.5$ mm, adherends thickness of $t_p = 3$ mm, the adhesive thickness of $t_A = 0.56$ mm and width of $B = 25$ mm (as shown in Figure 2).

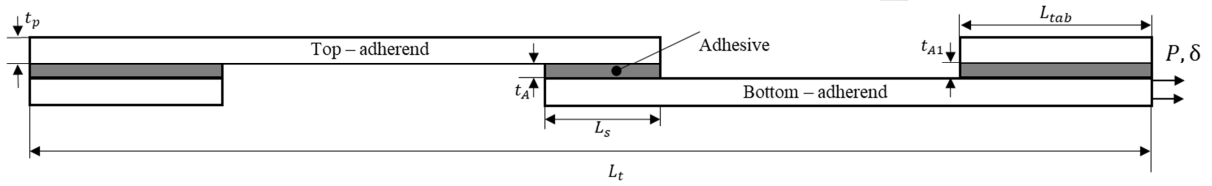


Figure 2: Geometry configuration of single-lap joint

The manufacturing of the specimens started by cutting aluminium and PPA plaques using disc cutter into the desired shape and length. To make sure a proper surface treatment, the bonding surfaces of both aluminium and PPA adherends were prepared by grit blasting (Guyson Grade 12 - Metallic Blast Media, corresponded to particles size of 150-250 microns) and cleaned with compressed air to remove the abrasive particles created by the blasting process. After this procedure, all the adherends were cleaned with Acetone and Loctite SF 706 in order to remove grease spots. Specific fixtures were manufactured to guarantee the alignment, control the adhesive thickness, control the overlap length and facilitate the preparation of a large number of samples. For DCB and ENF specimens, wires with diameters of 0.56 mm were located at the rear to provide a constant thickness of 0.56 mm, and a blade with a thickness of 0.1 mm was located at the edge of the adhesive layer to create a crack tip. The blade was positioned between two spacers with a thickness of 0.2 mm to ensure pre-crack at the mid-thickness of the adhesive layer. For TAST specimens, wires with a thickness of 3 mm were used to create the constant thickness of adhesive ($t_A = 3$ mm). The aluminium foil was located between two spacers with a thickness and height of 1.45 mm to create the initial crack length of $a_0 = 5$ mm at the left end of the overlap. Moreover, a wire with a thickness of $L_{gap} = 1.5$ mm was used to keep the gap between two adherends. End tabs with the length of $L_{tab} = 25$ mm were bonded to SLJ samples with epoxy adhesive with the thickness of $t_{A1} = 0.56$ mm to reduce the bending moment effect during the tests. The samples were left for curing under room temperature for seven days. Five specimens of each category were made, resulting in a total of 45 specimens for each adhesive.

2.3. Joints Testing

All mechanical tests were carried out using Instron 3380 with a 100 kN load cell. Non-contact optical measurement system (Imetrum) was used to measure crack length for DCB, ENF and TAST tests and displacements in SLJ tests (Figure 3). All specimens were masked using a white background and black dots with a diameter of 0.3 mm in order to create speckle patterns on the specimens' surface for the camera to be tracked. The first pattern was used as the reference image, which other images compared with it. A paper rule was used to calibrate the dimension in the camera. A paper rule was used to calibrate the dimension in the camera.

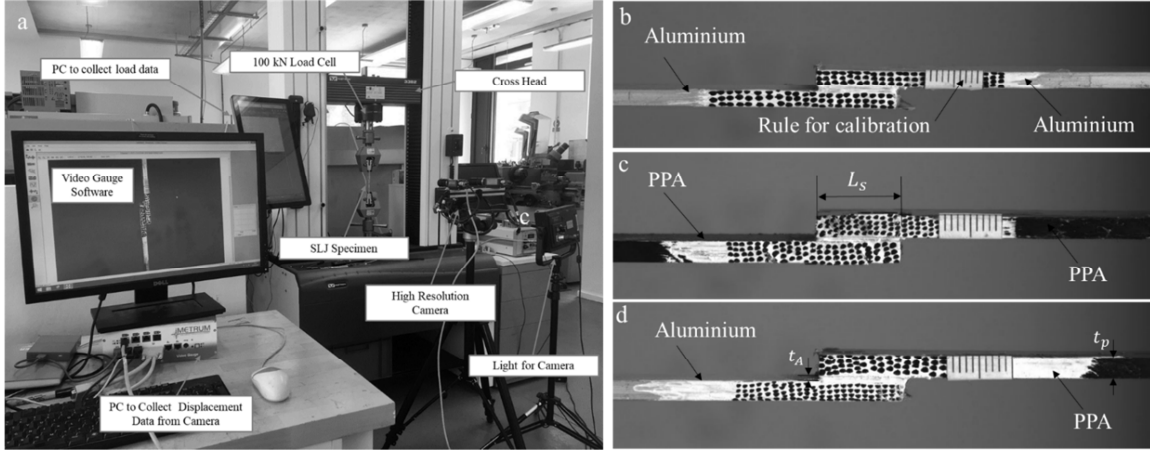


Figure 3: The tensile test setup for SLJ with non-contact measurement system (a) AL-AL SLJ (b) PPA-PPA SLJ (c) AL-PPA

3. Numerical Modelling

3.1. Cohesive parameters

Cohesive zone model (CZM) laws are based on a relationship between cohesive forces, and displacement jumps along the material surface, and it is one of the most commonly used methods that allows simulating the degradation and eventual failure of the adhesive bond-line. The adhesive bond-line behaves elastically until contact stress reached the nominal traction stress (t consists of two components (t_n and t_s) in two-dimensional in normal and shear directions respectively). The elastic behaviour can be written as follow:

$$\mathbf{t} = \begin{Bmatrix} t_n \\ t_s \end{Bmatrix} = \begin{bmatrix} E_{nn} & E_{ns} \\ E_{ns} & E_{ss} \end{bmatrix} \begin{Bmatrix} \delta_n \\ \delta_s \end{Bmatrix} = \mathbf{K}\delta$$

Where δ_n and δ_s are tensile and shear separations at the crack tip, respectively. The normal and tangential stiffness can be estimated: $E_{nn} = E/t$, $E_{ss} = G/t$, $E_{ns} = 0$ [16] (where E and G are Young's modulus and shear modulus, respectively and t is a cohesive zone thickness) to provide a reasonable stiffness and to avoid numerical problems. Once the damage initiation criterion is reached, the damage evolution describes the rate at which cohesive stiffness decreases as damage increases until the cohesive elements failed at the point where the relative displacement reached the limit value. There are two components that define damage evolution: the first component is energy dissipated due to failure, the values of G_{IC} and G_{IIC} are representing values under the traction separation laws in tension and shear directions, respectively. The second component is based on the nature of the damage variable, which is responsible for the softening section of the CZM law.

In this study, G_{IC} and t_n were measured by using J -integral (direct method) for all the AL-AL and PPA-PPA samples using DCB tests. For CZM parameters (G_{IIC} and t_s) in the shear direction, different approaches were implemented based on different adhesives types. For epoxy adhesive, the crack propagated too fast to be tracked during the tests. Consequently, the length of the crack and rotations at the crack tip cannot be measured accurately. Therefore, the compliance-based method (CBBM) was used for the calculation of G_{IIC} as it does not require the length of the crack. The traction in the shear direction (t_s) was determined by using the indirect method from the experimental data obtained from ENF tests by conducting 2D FE modelling with Abaqus[®]. For polyurethane adhesive, the fracture energy in the shear direction (G_{IIC}) was obtained by calculating J -integral at the maximum failure load by using the FEA code in Abaqus[®] as the adherends failed under high compressive load in the conventional ENF test, which arrested crack propagation. The t_s was calculated using the indirect method from TAST load-displacement data by using the FE model in Abaqus[®] [15]. Table 3 shows a summary of CZM parameters for both adhesives bonded with two different adherends. In order to have a consistent discussion in the FEA modelling section, the AL-AL adherends results represent the interface property between the AL and adhesives and the PPA-PPA adherends results represent the interface property between the PPA and adhesives.

Table 3: CZM parameters for two adhesives bonded with two different types of adherends

| Property | Terson MS 9399 (AL-AL adherends) | Terson MS 9399 (PPA-PPA adherends) | Loctite EA 9497 (AL-AL adherends) | Loctite EA 9497 (PPA-PPA adherends) |
|------------------|-------------------------------------|---------------------------------------|--------------------------------------|--|
| G_{Ic} (N/mm) | 2.11 ± 0.27 | 0.95 ± 0.12 | 0.26 ± 0.06 | 0.22 ± 0.04 |
| G_{IIC} (N/mm) | 6.5 ± 0.20 | 4.1 ± 0.50 | 0.90 ± 0.388 | 0.46 ± 0.090 |
| t_n (MPa) | 2.52 ± 0.45 | 0.65 ± 0.24 | 25.35 ± 10.263 | 20.94 ± 7.27 |
| t_s (MPa) | 6.67 ± 0.25 | 3.5 ± 0.20 | 16 ± 5 | 10 ± 3.75 |

In all cases, the mixed-mode behaviour of a power law with the average value of normal and shear CZM parameters was used to create triangular traction-separation laws embedded in the cohesive models for both adhesives. Although ductile adhesives are modelled with trapezoidal in literature, a triangular rather than trapezoidal traction rule was chosen due to a relatively linear relationship in a shear (TAST test) without a stress plateau [15]. As shown in Figure 4a, the values of τ_n and τ_s at the interface between PPA adherend and epoxy adhesives are smaller by 20 % and 37 % respectively, compared with the values for the interface with AL adherend and epoxy adhesive due to the higher stiffness of AL adherends, which leads to better stress distribution along bond-line. In general, the interface with epoxy adhesive has higher values of the tractions in both normal and shear directions compared with polyurethane adhesive regardless of the adherend, but the failure displacement is significantly lower than the value in the interface with polyurethane adhesive. This suggests that the joints with brittle adhesive are going to fails at the first sign of damage immediately after reaching stress softening in the damage law [10], while polyurethane adhesive allows plasticisation inside adhesive layer before failure.

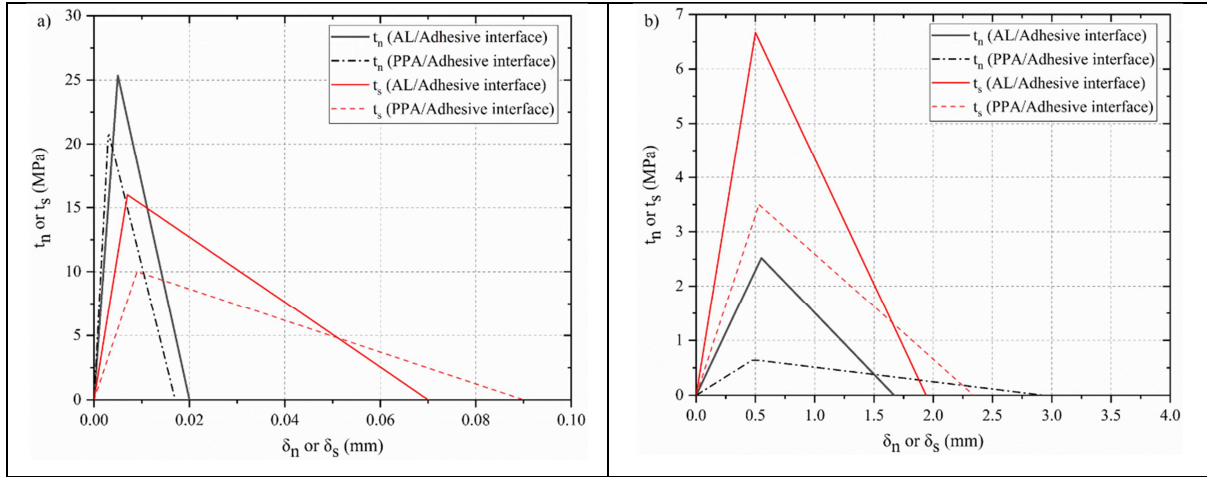


Figure 4: Cohesive laws for values of τ_n and τ_s in (a) epoxy (b) polyurethane adhesives for AL and PPA adherend

3.2. FEA Modelling

Two dimensional (2D) single-lap joint (SLJ) models with different adherends and adhesives were developed using Abaqus[®] to predict the strength and analyse stress distributions along with interfaces. In order to predict the strengths of the joints, six numerical models were built by using two different types of adherends and adhesives, as shown in Table 2. The adhesive layer was divided into three layers: two layers of cohesive elements element along the two interfaces (path 1 and 2) and one layer of continuum element in the middle section of the adhesive layer (Figure 5). The method allows defining different cohesive parameters to the individual interface according to its adjacent adherend (Table 3). The adherends and the middle section of the adhesive were meshed by 4-noded plane strain elements (CPE4R in Abaqus[®]) with four and two elements through-thickness, respectively. The cohesive layers were defined using the cohesive element (COH2D4 from Abaqus[®]) with a single element in the thickness direction and mesh size of 0.05 mm. All sections were meshed with a 0.2 mm mesh size along length after a mesh convergence study.

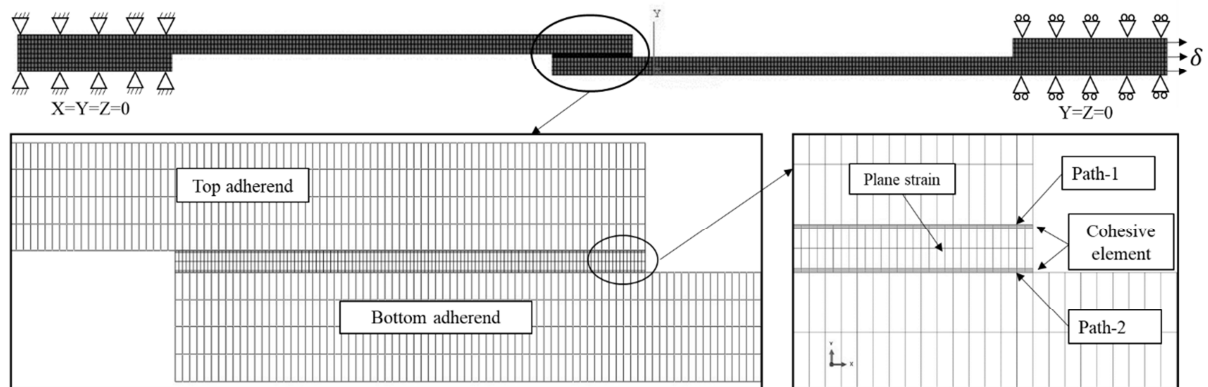


Figure 5: Mesh details of FE model

The higher mesh density was utilised for stress analysis to capture a more accurate stress gradient at the overlap edges. The adhesive section was meshed with plane strain element (CPE4R) with a size of 0.05 mm along the length in the bonding area and 12 and 15 elements were used through-thickness for adhesive and adherends, respectively. The single bias method was used for other sections of the

adherend to reduce the computational time. In order to simulate the single-lap test, the left end of the joint was fixed, and a horizontal displacement was applied to another end of the joint, as shown in Figure 5. Tie constraints were used to attach the cohesive elements to the substrate and the adhesive. All simulations were solved using the explicit solver of Abaqus[®] to compensate for the large deformation of polyurethane adhesive and the rapid crack growth along the bond line of the epoxy adhesive. Semi-automatic mass scaling of the whole model with the scale factor of 2 and 50 were used for models with polyurethane and epoxy adhesive respectively, after a convergence study compared to the load-displacement curves from the experiments. The smaller scale factor is used for polyurethane adhesive to capture post-failure (relatively gradual load drop) after maximum failure load. The developed cohesive laws (Figure 4) were used in the simulation. Table 4 shows the combination of the cohesive layers for single-lap joints. Path-1 has the cohesive property between the adhesive and top adherend, and path-2 has the cohesive property between adhesive and bottom adherend. The AL-AL and PPA-PPA joints have the same cohesive property in path 1, and 2 as the top and bottom adherends were made of the same material, but in the AL-PPA joint path 1 has the property of the AL/adhesive interface properties, and path 2 has the PPA/adhesives interface property.

Table 4: The combination of the cohesive layers for the Single-lap joints

| ID | Path 1 (Interface Property) | Path-2 (Interface Property) |
|----------------|------------------------------------|------------------------------------|
| AL-AL | AL/adhesive | AL/adhesive |
| AL-PPA | AL/adhesive | PPA/adhesive |
| PPA-PPA | PPA/adhesive | PPA/adhesive |

Due to the high viscosity of the polyurethane adhesive, a hyper-elastic model was required for simulations to adapt the large deformation of the adhesive. Different hyperplastic constitutive models were tested in Abaqus[®] using the experimental results to find the best curve fitting for the stress-strain curves. The Arruda-Boyce model was selected as the most suitable one. Table 5 presents Arruda-Boyce parameters for polyurethane adhesive, with all these parameters as inputs for FE modelling.

Table 5: Arruda-Boyce parameters for polyurethane

| Arruda-Boyce parameters | | | | |
|-------------------------|----------|-----------|---------|------------------|
| Parameters | Mu (MPa) | mu-0(MPa) | LAMBDA | D (MPa^{-1}) |
| Average | 1.016 | 1.04 | 1867.76 | 0.152 |

4. Results and discussion

4.1. Load vs displacement of single-lap joint

Five SLJ specimens of each design category were tested under tensile load, and three representative results were presented in the below figures. Figure 6 and 7 present comparisons between experimental and numerical results for the joints with epoxy and polyurethane adhesives, respectively. In general, there are good agreements between experimental and numerical results.

The results show that the maximum failure load in samples with epoxy adhesive is more sensitive to the stiffness of adherends due to higher peak stress and instability in damage propagation. It is clear

from Figure 6 that the higher failure load achieved by the AL-AL joints rather than the PPA-PPA or AL-PPA joints. The maximum failure load of the SLJ decreases from approximately 3600 N to approximately 2500 N by changing both adherends from the AL to PPA, which corresponds to a 30.55% reduction in the joint strength. This is due to a larger bending and longitudinal deformation, which leads to higher stress concentrations at the overlap edges of the SLJs with lower stiffness adherend. The maximum failure loads for the AL-PPA and PPA-PPA joints are close to each other as the less stiff material determines joint strength in dissimilar joint scenarios [4]. The AL-PPA joint outperforms the PPA-PPA joint due to the existence of the AL adherend, which increases the overall stiffness of the joint that leads to a slightly smaller longitudinal displacement (0.3 mm for the AL-PPA joint and 0.4 mm for the PPA-PPA joint). The AL-PPA could not perform as well as the AL-AL joint due to asymmetric stress distribution along the bond line caused by the difference in the stiffness of both adherends, which leads to the higher shear stress concentration along with the interface of the adherend with lower stiffness (shown in Figure 10).

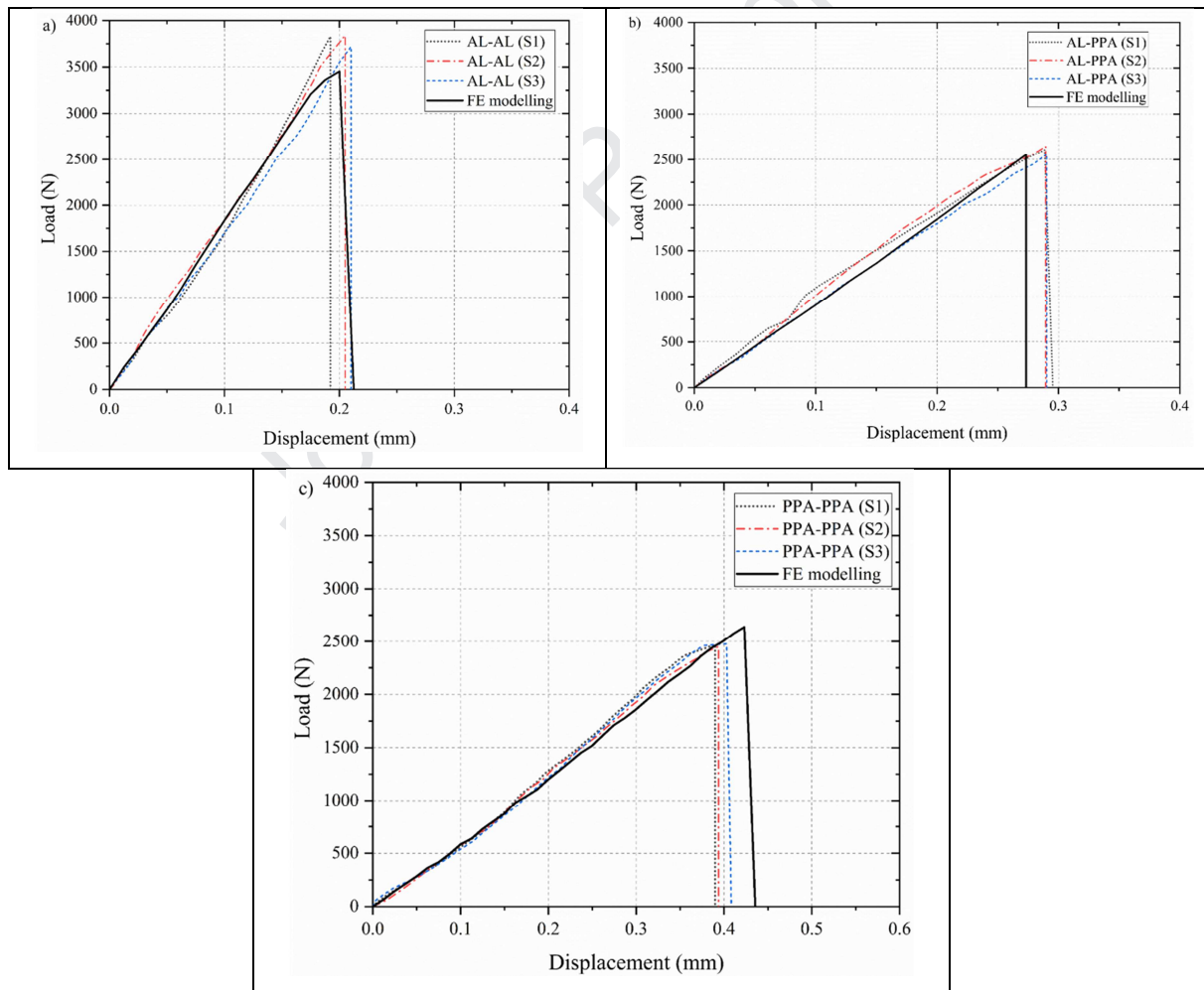


Figure 6: Load-displacement curves of (a) AL-AL, (b) AL-PPA and (c) PPA-PPA joints with epoxy adhesive

For SLJs with polyurethane adhesive, the stiffness of adherends does not play a significant role in the maximum failure load due to the large deformation of the adhesive and the stable damage growth

during loading. The magnitudes of the loads for the PPA-PPA and the AL-PPA joints are 6.18% and 2.86% lower compared to the one of AL-AL joint (Figure 7). The maximum displacement of the joints with polyurethane adhesive is significantly larger than the one of the joints with epoxy adhesive (0.2 mm for the AL-AL joint with epoxy adhesive and 2 mm for the AL-AL joint with polyurethane adhesive). This is due to the plasticisation allowance of the polyurethane adhesive before its failure [7], while epoxy adhesive does not allow any plasticisation and fails at the first sign of the crack at the corners [17]. It is observed for an epoxy adhesive that the displacement at failure in the PPA-PPA and the AL-PPA joints are approximately double with respect to the AL-AL joints due to lower stiffness of the PPA substrates. On the other hand, all the joints with polyurethane adhesive fail at a similar displacement (approximately 2 mm) as the polyurethane adhesive contributes most of the overall deformation.

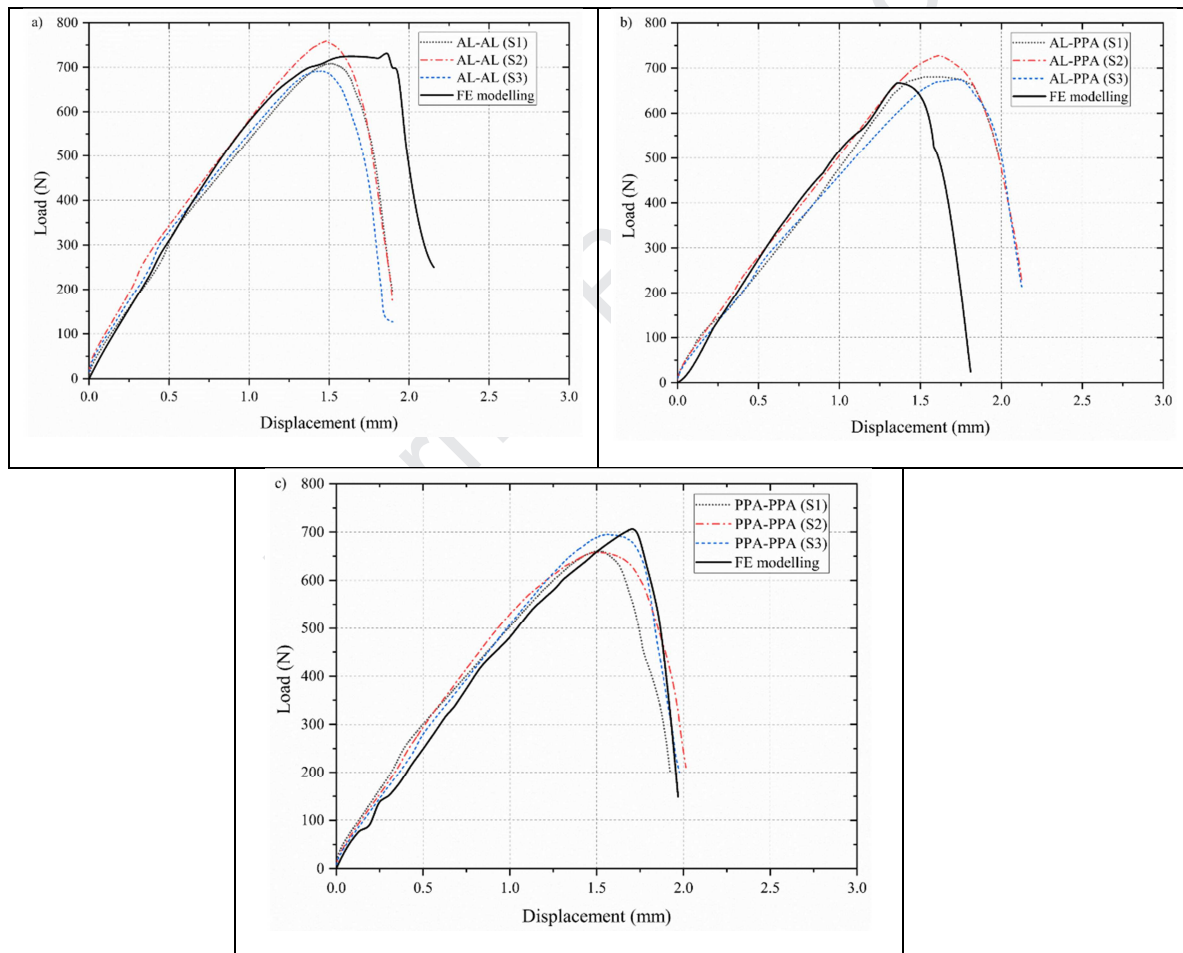


Figure 7: Load-displacement curves of (a) AL-AL, (b) AL-PPA and (c) PPA-PPA joints with polyurethane adhesive

Figure 8 indicates the failure loads of hybrid joints when different cohesive parameters are used for both adhesives. Three different numerical models of the AL-PPA joint are utilised with three different groups of CZM parameters. The first model (named as AL-PPA-1) uses hybrid cohesive properties, which defines path 1 using the AL/adhesive parameters and path 2 using the PPA/adhesive parameters, respectively (Table 6). For the AL-PPA-2 and AL-PPA-3 models, identical CZM

parameters are used in paths 1 and 2. AL-adhesive parameters are used for the AL-PPA-2 model, and PPA-adhesive parameters are used for the AL-PPA-3 model to define the cohesive zone in the bonding area.

Table 6: Different CZM parameters for the AL-PPA joint

| ID | Path 1 (Interface Property) | Path-2 (Interface Property) |
|----------|-----------------------------|-----------------------------|
| AL-PPA-1 | AL/adhesive | PPA/adhesive |
| AL-PPA-2 | AL/adhesive | AL/adhesive |
| AL-PPA-3 | PPA/adhesive | PPA/adhesive |

As shown in Figure 8, the simulation results obtained from the AL-PPA-1 achieves good agreements with the experimental results. For the maximum failure load, the differences between numerical and experimental results are 0.738 % and 0.43% for the joints with epoxy and polyurethane adhesives, respectively. On the other hand, for the joint with identical CZM parameters from the AL/adhesive interface in both paths 1 and 2 (AL-PPA-2), the differences between numerical and experimental results increase to 14.12% when the adhesive is epoxy and 18.27 % when the adhesive is polyurethane. For the joint with identical CZM parameters of the PPA/adhesive interface (AL-PPA-3), the differences between the numerical and experimental results are 4.6 % and 15% for the joints with epoxy and polyurethane adhesives, respectively. It can be seen from the simulation results that the model (AL-PPA-1) with the hybrid cohesive parameters gives the best simulation results and the results from model AL-PPA-3 are more accurate than the results of the model AL-PPA-2. The result reveals that the strength of the hybrid joint is dominated by the properties of the interface adjacent to the adherend with lower stiffness, which is the interface between PPA and the adhesive in this study.

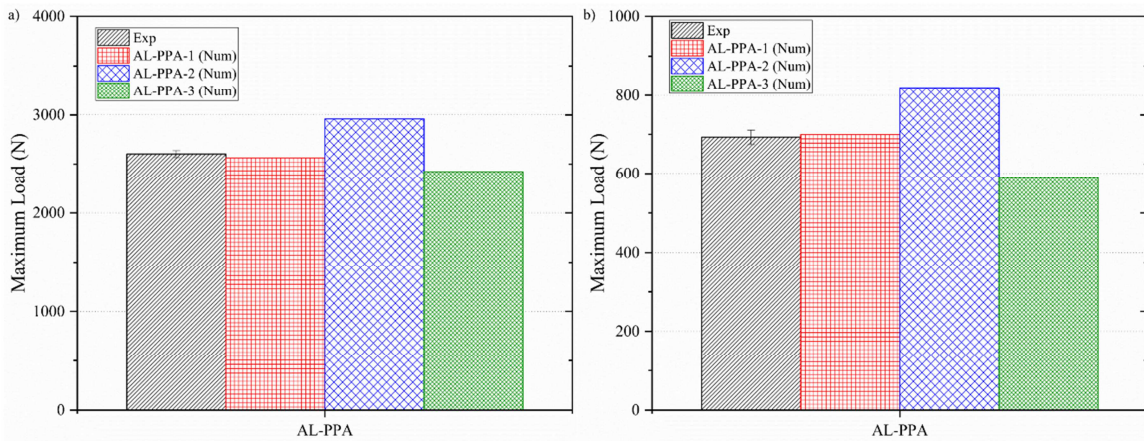


Figure 8: The effect of different CZM parameters for hybrid (AL-PPA) joints with (a) epoxy and (b) polyurethane adhesives

4.2. Effect of the stiffness of adherends and adhesives on the rotation of SLJ

The rotations of the over-lap region of the single-lap joints were studied to understand the effects of the stiffness of the adherends on the deformation mechanism of the joints. The rotation of a joint generates excessive stresses at the ends of the overlap in the substrates, which results in adherends yielding and the fracture initiation in the adhesive layer [18], [19]. Three different single-lap joint designs (AL-AL, AL-PPA, and PPA-PPA) with two different adhesives (epoxy and polyurethane) were used in the analysis. The rotations were measured using a non-contact method by defining the

three reference lines: A-B, C-D, and E-F (Figure 9). The rotations of the lines represent the rotations of the adherend-1, adherend-2 and the adhesive layer, respectively. For instance, the following formula was used to calculate rotation in each section:

$$\theta = \cos^{-1} \frac{\overline{AB} \cdot \overline{A'B'}}{|\overline{AB}| |\overline{A'B'}|}$$

where \overline{AB} and $\overline{A'B'}$ are vectors representing the initial position of the reference line AB and the position of the line after rotating; $|\overline{AB}|$ and $|\overline{A'B'}|$ are the length of the vectors.

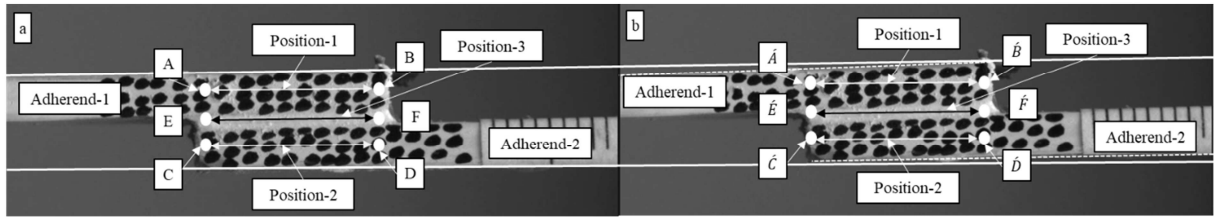


Figure 9: Non-contact measurement of rotation at (a) initial position and (b) after the rotation

Table 7 shows the rotations of the single-lap joints under their maximum loads with different combinations of constituents. For the joints with the same adhesives, the AL-AL joint generally has a smaller degree of rotation in all three positions (rotations 1-3) comparing with the PPA-PPA and the AL-PPA joints. The only exception is the rotation of adherend 1 (rotation-1) in the joint with polyurethane adhesive, the degree of rotation of the AL-AL joint is slightly higher (8.3%) than the one of AL-PPA joint. The phenomenon indicates that the high stiffness adherends provide higher global rigidity in the joint, which results in smaller global rotation [5]. For instance, the degree of rotation in the PPA-PPA joint is 94.95% and 74.35% higher than the magnitudes of rotation in the AL-AL joint, when the adhesive is epoxy and polyurethane, respectively.

In addition, similar degrees of rotations are obtained from all three positions of the joints with identical adherends (AL-AL and PPA-PPA) and the same adhesive. For instance, the magnitudes are 1.19, 1.2 and 1.17 degrees in positions 1, 2, and 3, respectively, for the AL-AL joint with epoxy adhesive. However, the degrees of rotations are different in various positions in the hybrid joint (AL-PPA). The magnitudes are 1.54, 1.85 and 1.75 degrees in positions 1, 2 and 3 when the adhesive is epoxy. This can be explained due to significant bending moment in the adherend when using lower stiffness material (PPA side). It also partially explains that the failure of the hybrid joint tends to occur along with the PPA/adhesive interface, which is observed in both experimental and numerical analysis. Beside the stiffness of adherend, the stiffness of the adhesive also affects the rotation of the single-lap joint. Single-lap joints with polyurethane adhesives have a smaller degree of rotation compared with the joints with epoxy adhesive, which is shown in Table 7. This is due to the relatively low stiffness and elastic properties of the polyurethane adhesive.

Table 7: Rotations in single-lap joints with different combinations of constituents

| ID | Position-1 (degree) | | Position-2 (degree) | | Position-3 (degree) | |
|---------|---------------------|--------------|---------------------|--------------|---------------------|--------------|
| | Epoxy | polyurethane | Epoxy | polyurethane | Epoxy | polyurethane |
| AL-AL | 1.19 | 0.39 | 1.2 | 0.4 | 1.17 | 0.49 |
| AL-PPA | 1.54 | 0.36 | 1.85 | 0.64 | 1.75 | 0.60 |
| PPA-PPA | 2.32 | 0.68 | 2.36 | 0.71 | 2.30 | 0.68 |

4.3. Stress distribution

Stress analysis was performed to assess the influence of the stiffness of the constituents on the peel (σ) and shear (τ) stresses along with the adhesive layer based on the developed FE models. All stress distributions were obtained along the neutral axis of the adhesive layer. Displacements of 0.1 and 0.4 mm were applied for the joints with epoxy and polyurethane, respectively when the deformation of the joints is elastic. The peel and shear stresses were normalised by the average shear stress (τ_{avg}), and the bond-line length was normalised (x/L_s) by the total length of the overlap (L_s). Based on the trend of the distribution, the overlap was divided into three sections: at the corners $0 < x < 0.1$ (section-I), $0.9 < x < 1$ (section-III) and the overlap inner region $0.1 < x < 0.9$ (section-II).

As shown in Figure 10a, the peel stress of the joints with epoxy adhesive is generally low, and uniform in section II of the bond-line and high-stress levels are obtained at sections I and III, which locates at the ends of the overlap. This can be justified by adherends rotation that results in high peak stress in those areas [20]. The shear stress follows the same tendency (Figure 10 b), with lower stresses at the inner region (section II) of the bond-line and higher stresses at the ends because of the free edge effects of the adhesive layer [21]. For the joints with identical adherends (AL-AL and PPA-PPA), the stress distributions are symmetric along the overlap. The PPA-PPA joint has the relative highest peak stresses (σ/τ_{avg} and τ/τ_{avg}) at both ends of the overlap (sections I and III) due to the lower stiffness of the adherends, which results in a larger bending at the overlap area. Comparing with the AL-AL joint, the peak σ/τ_{avg} and τ/τ_{avg} values are 40% and 43% higher, respectively.

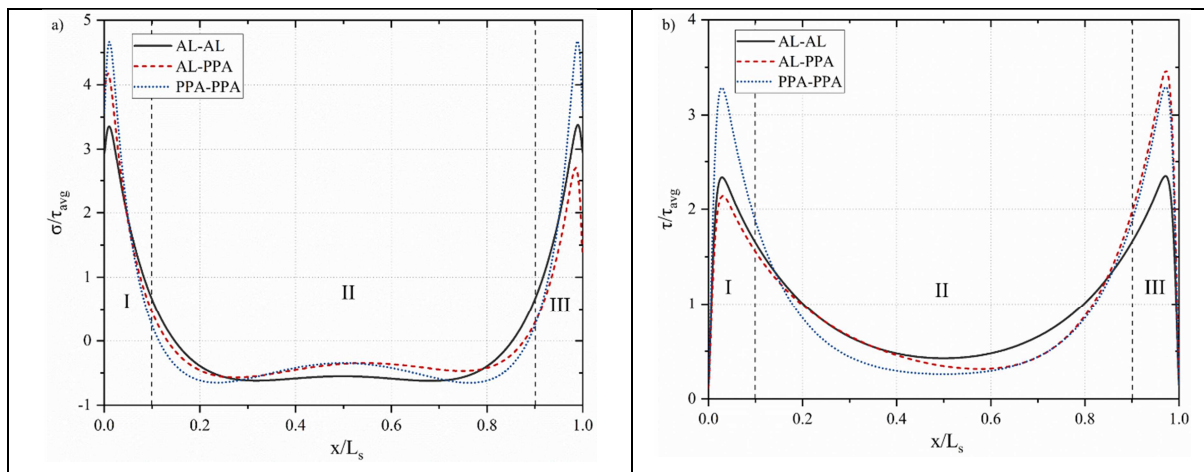


Figure 10: (a) Peel and (b) Shear distribution of the AL-AL, AL-PPA and the PPA-PPA joints with an epoxy adhesive

For the joints with polyurethane adhesive (Figure 11 a and b), both the peel and shear stress distributions are uniform along the bond-line, when the joints consist of identical adherends. This is due to the hyper-elastic property of the adhesive, which leads to higher compliance of the adhesive layer compared with the epoxy adhesive. The peak values of stresses at the ends of the overlap (sections I and III) are significantly lower in comparison to the joints with epoxy adhesive. For instance, in the AL-AL joints with polyurethane adhesive, the peel (σ/τ_{avg}) and the shear stress (τ/τ_{avg}) are lower by 77.82% and 56.08%, respectively compared to the AL-AL joint with epoxy adhesive.

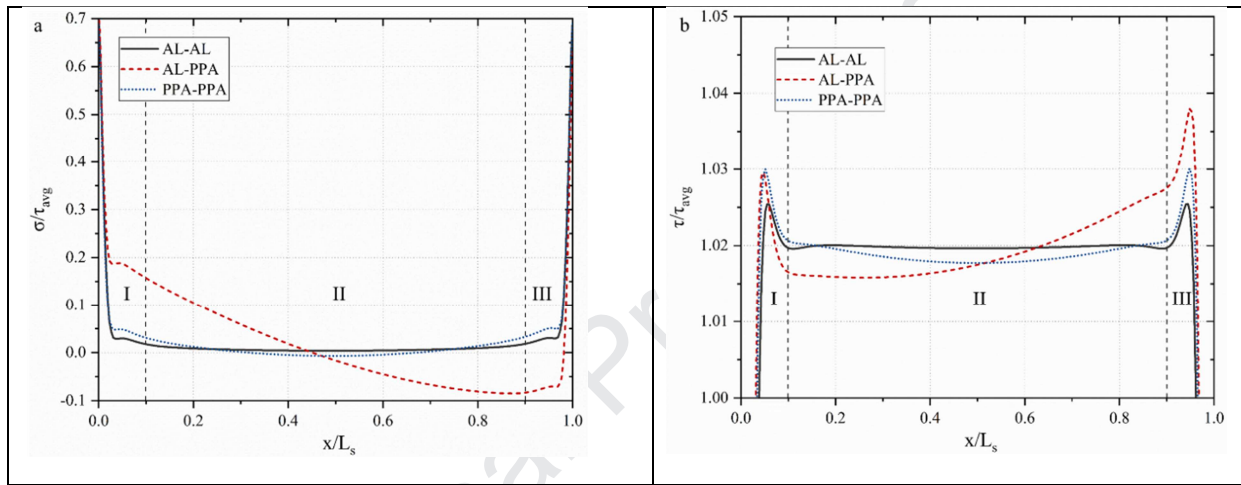


Figure 11: (a) Peel and (b) Shear distribution of the AL-AL, AL-PPA and the PPA-PPA joints with a polyurethane adhesive

Asymmetric stress distributions are observed in the hybrid joint (AL-PPA) due to the stiffness mismatch of the adherends, as shown in Figure 10 and 11, which lead to different longitudinal deformations at the overlap edges. For the AL-PPA joint with an epoxy adhesive (Figure 10 a), the peak value of the σ/τ_{avg} in section-I (AL side) is higher by 34.54% compared to section-III (PPA side). This is due to the increase of the longitudinal deformation of PPA adherend. Since the aluminium adherend experiences smaller longitudinal deformation, the higher peak value of the σ/τ_{avg} is developed toward section-I. The same trend is also found in the AL-PPA joint with polyurethane adhesive (Figure 11 a). However, the difference of the values of the peak stresses is lower than the joint with epoxy adhesive, which is caused by the lower stiffness and hyper-elastic properties of the polyurethane adhesive.

The asymmetric distributions of shear stress are also observed in the analysis. For the joints with epoxy adhesive (Figure 10 b), the peak shear stress of the AL-PPA joint in section I is close to the stress of the AL-AL joint with a slightly 10.24% difference. This is due to the identical adherends at this end of the joints. However, the peak shear stress of the AL-PPA joint in section III is significantly higher than the one of the AL-AL joint by 47.86% which is due to the different stiffness of the adherends at this end of the joint. The same tendency is observed for the joints with polyurethane

adhesive, though the effect of asymmetric stress distribution is reduced due to the high ductility of the adhesive. The asymmetric distribution of shear stress of the hybrid joint can be used to explain its failure mode. According to the results of both experiments and numerical simulation (Figure 14), the damage of hybrid joints usually initiates at section III and along with the interface between the adhesive and the adherend with lower stiffness, which could be mainly affected by the higher shear stress concentration.

4.4. Stiffness degradation (SDEG)

The SDEG represents the overall scalar stiffness degradation of the cohesive element, and the value has the range from 0 (undamaged material) to 1 (entirely failed). In this analysis, the SDEG variables were plotted at two instances: (1) when the first CZM failure occurs and (2) when the maximum load was attained. For the joint with identical adherend (AL-AL and PPA-PPA), the SDEG values along path 1 and path 2 are the same due to the symmetric stress distribution. Hence the plot along path 1 was used in the analysis as a representative. For the hybrid joint (AL-PPA), the values of SDEG along both path 1 (AL/adhesive interface) and path 2 (PPA/adhesive interface) were plotted separately. The SDEG plots for the joints with epoxy and polyurethane adhesive are shown in Figure 12 and 13, respectively. For the joints with epoxy adhesive, the proportions of the overlap under damage for the AL-AL and PPA-PPA joints are 5.2% and 4.1%, respectively, when the failure initiates (Figure 12 a). When load achieves the maximum failure load, the proportion under damage is 16.4% for the AL-AL joint and 9.5% for the PPA-PPA joint (Figure 12 b). The AL-AL joint has a wider degradation area compared to the PPA-PPA joint. This can be justified by lower stress concentrations at sections I and III in the overlap of the AL-AL joint, due to the higher stiffness of the AL material.

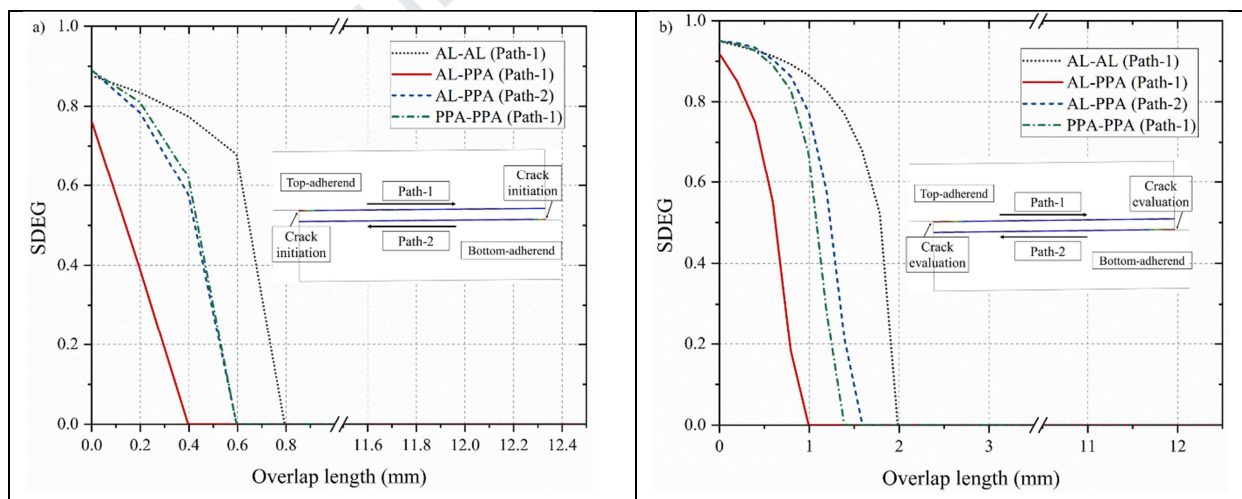


Figure 12: (a) SDEG of AL-AL, AL-PPA and PPA-PPA joints with an epoxy adhesive (a) when first CZM element damaged (b) under the maximum load point

For the joints with identical adherends bonded with polyurethane adhesive, the value of SDEG is generally lower than the joints with epoxy adhesive, when the damage initiates (Figure 13 a). For instance, the SDEG value for the AL-AL joint with epoxy adhesive is 0.95, while this value is 0.65 for the AL-AL joint with the polyurethane adhesive. This is due to the lower strength of polyurethane

compared with epoxy, namely lower values of t_n and t_s , and higher values of G_{IC} and G_{IIC} (Table 3). When load achieves the maximum failure load, the joint with polyurethane spread damage in a more extensive area, with the total area under the damage of 28.3 % for the AL-AL joint and 17.4% for the PPA-PPA joint (Figure 13 b). The results show that SDEG spreads further within the bond-line with the increasing adhesive ductility.

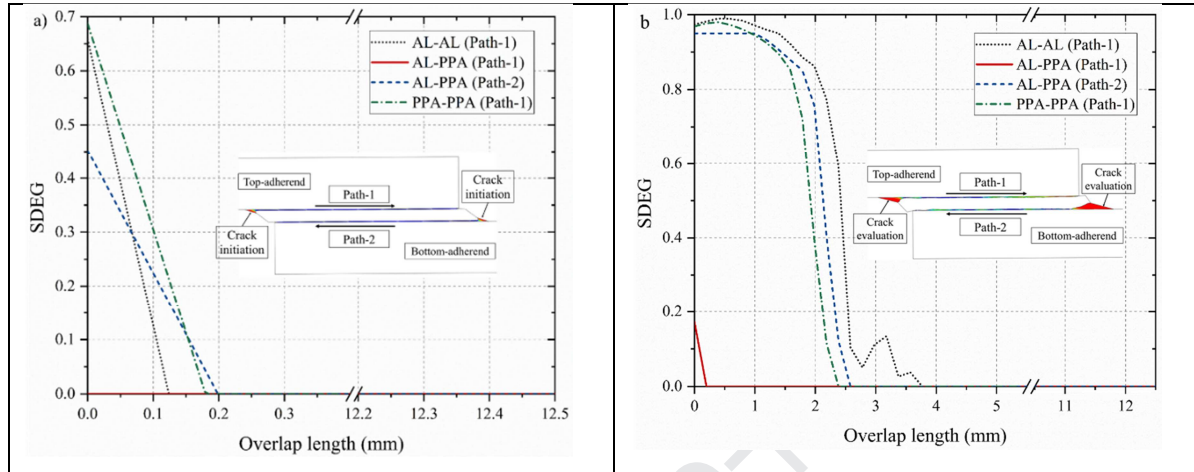


Figure 13: (a) SDEG of AL-AL, AL-PPA and PPA-PPA joints bonded with a polyurethane adhesive (a) when first CZM element damaged (b) under the maximum load point

For the hybrid joint (AL-PPA), The SDEG plot is unsymmetrical along paths 1 and 2. This is due to the differences in the stiffness of the adherends. At the instant the first CZM element fails, the damage spreads by 4.7% along path 2 (PPA side) and 3.1% along path 1 (AL side), when the adhesive is epoxy (Figure 12 a). For the joint with polyurethane adhesive (Figure 13 a), the damage along path 2 is 2%, while path 1 stays undamaged (SDEG=0). This means that the crack initiation in the hybrid joint occurs along path 2, which is the interface between with lower stiffness adherend (PPA) and adhesive. The phenomenon can be observed in both the experimental and numerical results, as shown in Figure 14. When the maximum failure load occurs, the damage extends 12.3% and 7.4% along path 2 and path 1 of the joint with epoxy adhesive. It shows both interfaces (Path 1 and 2) have damage, although the damage along Path 2 dominates the overall failure. For the joints with polyurethane adhesive, the damage is 21% along path 2 and 2% along paths 1. The results show that the failure of the hybrid joint only occurs along with the interface adjacent to the low stiffness adherend.

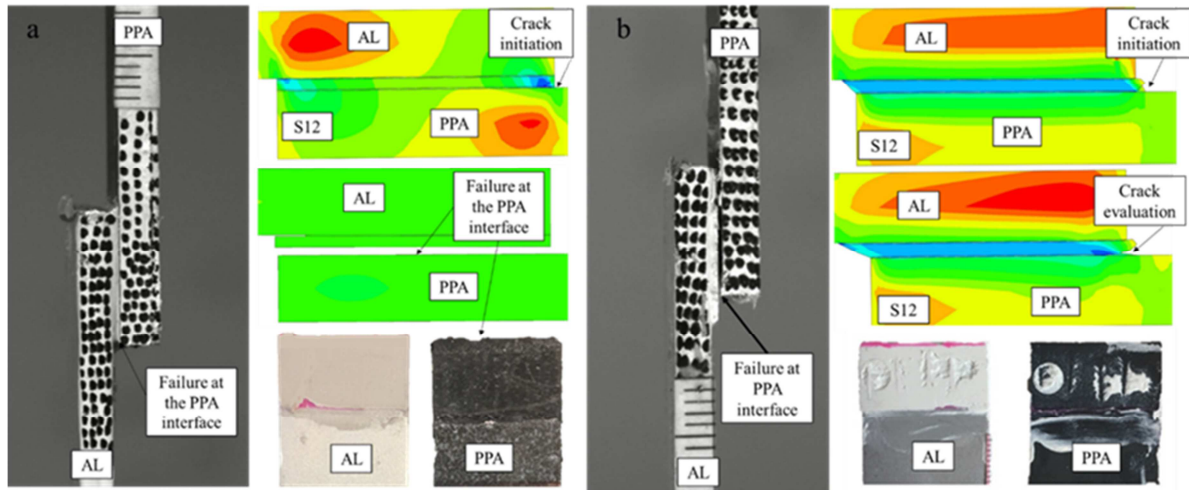


Figure 14: The failure process in AL-PPA joints for (a) epoxy and (b) polyurethane adhesives

5. Conclusion:

In this work, the effects of the stiffness of the constituents of an adhesive joint on its fracture mechanism were studied. Joints with different combinations of adherends and adhesives were analysed using both numerical and experimental methods. According to the analysis of the results, the following conclusions could be summarised:

- A novel FE model is developed to describe the mechanical performance of the adhesive joint by introducing two layers of the cohesive element at the individual interfaces. The method allows defining different cohesive parameters to the interfaces according to the adjacent adherend. It is especially suitable to simulate hybrid joints with interfacial failure. It is superior to the conventional method, which considers the overall adhesive layer as one cohesive zone.
- The load vs displacement behaviour of the single-lap joints demonstrate that the stiffness of adherend affects the maximum failure load of the joints with rigid adhesive (epoxy). The value of the AL-AL joint is higher than the hybrid joint (AL-PPA) and the PPA-PPA joint. In addition, it is observed that the overall displacement of the AL-AL is only half of the value of the PPA-PPA joint, which is also due to the different stiffness of adherends. For the joint with flexible adhesive (polyurethane), the maximum failure load is not sensitive to the stiffness of the adherend as the joints with different combinations of adherends have similar maximum failure loads. Moreover, the overall displacements of the joints are also similar. This can be explained as the mechanical behaviours of the joints are determined by the mechanical properties of the adhesive rather than the adherend.
- For the joint with identical adherend, the stress distributions along the bond-line are symmetric. For the hybrid joint, the asymmetric stress distribution is obtained due to the mismatch stiffness of the adherends. This determines the failure mode of the joint. Higher shear stress distribution occurs in the interface adjacent to the adherend with lower stiffness

(PPA). This dominates the fracture initiation in the case studies regardless of the adhesive types. In addition, the adhesive with lower stiffness and higher ductility effectively reduces the stress concentrations at the ends of the bond-line and the effects of asymmetric stress distributions.

References:

- [1] Z. J. Wu, A. Romeijn, and J. Wardenier, "Stress expressions of single-lap adhesive joints of dissimilar adherends," *Compos. Struct.*, vol. 38, no. 1–4, pp. 273–280, May 1997, doi: 10.1016/S0263-8223(97)00062-7.
- [2] T. Sawa, J. Liu, K. Nakano, and J. Tanaka, "Two-dimensional stress analysis of single-lap adhesive joints of dissimilar adherends subjected to tensile loads," *J. Adhes. Sci. Technol.*, vol. 14, no. 1, pp. 43–66, 2000, doi: 10.1163/156856100742104.
- [3] A. M. G. Pinto, A. G. Magalhães, R. D. S. G. Campilho, M. F. S. F. de Moura, and A. P. M. Baptista, "Single-Lap Joints of Similar and Dissimilar Adherends Bonded with an Acrylic Adhesive," *J. Adhes.*, vol. 85, no. 6, pp. 351–376, May 2009, doi: 10.1080/00218460902880313.
- [4] P. N. B. Reis, J. A. M. Ferreira, and F. Antunes, "Effect of adherend's rigidity on the shear strength of single lap adhesive joints," *Int. J. Adhes. Adhes.*, vol. 31, no. 4, pp. 193–201, Jun. 2011, doi: 10.1016/j.ijadhadh.2010.12.003.
- [5] A. M. Pereira, J. M. Ferreira, F. V. Antunes, and P. J. Bártolo, "Analysis of manufacturing parameters on the shear strength of aluminium adhesive single-lap joints," *J. Mater. Process. Technol.*, vol. 210, no. 4, pp. 610–617, Mar. 2010, doi: 10.1016/j.jmatprotec.2009.11.006.
- [6] L. F. M. da Silva, T. N. S. S. Rodrigues, M. A. V Figueiredo, M. F. S. F. de Moura, and J. A. G. Chousal, "Effect of Adhesive Type and Thickness on the Lap Shear Strength," *J. Adhes.*, vol. 82, no. 11, pp. 1091–1115, Nov. 2006, doi: 10.1080/00218460600948511.
- [7] S. L. S. Nunes, R. D. S. G. Campilho, F. J. G. da Silva, C. C. R. G. de Sousa, T. A. B. Fernandes, M. D. Banea, and L. F. M. da Silva, "Comparative Failure Assessment of Single and Double Lap Joints with Varying Adhesive Systems," *J. Adhes.*, vol. 92, no. 7–9, pp. 610–634, Sep. 2016, doi: 10.1080/00218464.2015.1103227.
- [8] Y. Zhu, K. M. Liechti, and K. Ravi-Chandar, "Direct extraction of rate-dependent traction–separation laws for polyurea/steel interfaces," *Int. J. Solids Struct.*, vol. 46, no. 1, pp. 31–51, Jan. 2009, doi: 10.1016/J.IJSOLSTR.2008.08.019.
- [9] A. Rudawska, "Adhesive joint strength of hybrid assemblies: Titanium sheet-composites and aluminium sheet-composites—Experimental and numerical verification," *Int. J. Adhes. Adhes.*, vol. 30, no. 7, pp. 574–582, Oct. 2010, doi: 10.1016/j.ijadhadh.2010.05.006.
- [10] D. L. Alves, R. D. S. G. Campilho, R. D. F. Moreira, F. J. G. Silva, and L. F. M. da Silva, "Experimental and numerical analysis of hybrid adhesively-bonded scarf joints," *Int. J. Adhes. Adhes.*, vol. 83, pp. 87–95, Jun. 2018, doi: 10.1016/j.ijadhadh.2018.05.011.
- [11] I. Katsivalis, O. T. Thomsen, S. Feih, and M. Achintha, "Development of cohesive zone models for the prediction of damage and failure of glass/steel adhesive joints," *Int. J. Adhes. Adhes.*, vol. 97, no. November, p. 102479, Mar. 2020, doi: 10.1016/j.ijadhadh.2019.102479.
- [12] J. Wang and P. Qiao, "Fracture Toughness of Wood—Wood and Wood—FRP Bonded Interfaces Under Mode-II Loading," *J. Compos. Mater.*, vol. 37, no. 10, pp. 875–897, May 2003, doi: 10.1177/0021998303037010002.

- [13] V. Tvergaard, "Resistance curves for mixed mode interface crack growth between dissimilar elastic-plastic solids," *J. Mech. Phys. Solids*, vol. 49, no. 11, pp. 2689–2703, Nov. 2001, doi: 10.1016/S0022-5096(01)00074-6.
- [14] D. . Packham, "Surface energy, surface topography and adhesion," *Int. J. Adhes. Adhes.*, vol. 23, no. 6, pp. 437–448, Jan. 2003, doi: 10.1016/S0143-7496(03)00068-X.
- [15] K. Hasegawa, A. D. Crocombe, F. Coppuck, D. Jewel, and S. Maher, "Characterising bonded joints with a thick and flexible adhesive layer-Part 1: Fracture testing and behaviour," *Int. J. Adhes. Adhes.*, vol. 63, pp. 124–131, 2015, doi: 10.1016/j.ijadhadh.2015.09.003.
- [16] R. D. S. G. Campilho, M. D. Banea, A. M. G. Pinto, L. F. M. da Silva, and A. M. P. de Jesus, "Strength prediction of single- and double-lap joints by standard and extended finite element modelling," *Int. J. Adhes. Adhes.*, vol. 31, no. 5, pp. 363–372, Jul. 2011, doi: 10.1016/J.IJADHADH.2010.09.008.
- [17] J. O. S. Silva, R. D. S. G. Campilho, and R. J. B. Rocha, "Crack growth analysis of adhesively-bonded stepped joints in aluminium structures," *J. Brazilian Soc. Mech. Sci. Eng.*, vol. 40, no. 11, p. 540, Nov. 2018, doi: 10.1007/s40430-018-1466-0.
- [18] G. Fessel, J. G. Broughton, N. A. Fellows, J. F. Durodola, and A. R. Hutchinson, "Evaluation of different lap-shear joint geometries for automotive applications," *Int. J. Adhes. Adhes.*, vol. 27, no. 7, pp. 574–583, Oct. 2007, doi: 10.1016/j.ijadhadh.2006.09.016.
- [19] E. F. Karachalios, R. D. Adams, and L. F. M. da Silva, "Single lap joints loaded in tension with ductile steel adherends," *Int. J. Adhes. Adhes.*, vol. 43, pp. 96–108, Jun. 2013, doi: 10.1016/j.ijadhadh.2013.01.017.
- [20] B. Zhao, Z.-H. Lu, and Y.-N. Lu, "Two-dimensional analytical solution of elastic stresses for balanced single-lap joints—Variational method," *Int. J. Adhes. Adhes.*, vol. 49, pp. 115–126, Mar. 2014, doi: 10.1016/j.ijadhadh.2013.12.026.
- [21] W. Jiang and P. Qiao, "An improved four-parameter model with consideration of Poisson's effect on stress analysis of adhesive joints," *Eng. Struct.*, vol. 88, pp. 203–215, Apr. 2015, doi: 10.1016/j.engstruct.2015.01.027.

Appendix

Figure 1 shows the average G_{IC} values obtained from the AL-AL and the PPA-PPA single-mode coupon specimens (DCB) for two different adhesives. In general, compliance-based (CBT, ECM, MCC) and J-integral methods have similar results (Less than 10% difference). For epoxy adhesive, the average G_{IC} value for the AL-AL specimens is estimated 7.40% lower in the J-integral method in comparison to the CBT method (0.28 N/mm). On the other hand, the estimated average G_{IC} value for the PPA-PPA specimens with the J-integral method is higher by 22.20% in comparison to CBT method (0.175 N/mm). For polyurethane adhesive, the average G_{IC} value for the AL-AL and the PPA-PPA specimens are higher by 8.43% and 3.20%, respectively, in J-integral method compared to the CBT method (1.93 N/mm for the AL-AL specimen and 0.92 N/mm for the PPA-PPA specimen). Due to the reasonable agreements between fracture energy values with different methods, the J-integral method was used to estimate the traction in the normal direction.

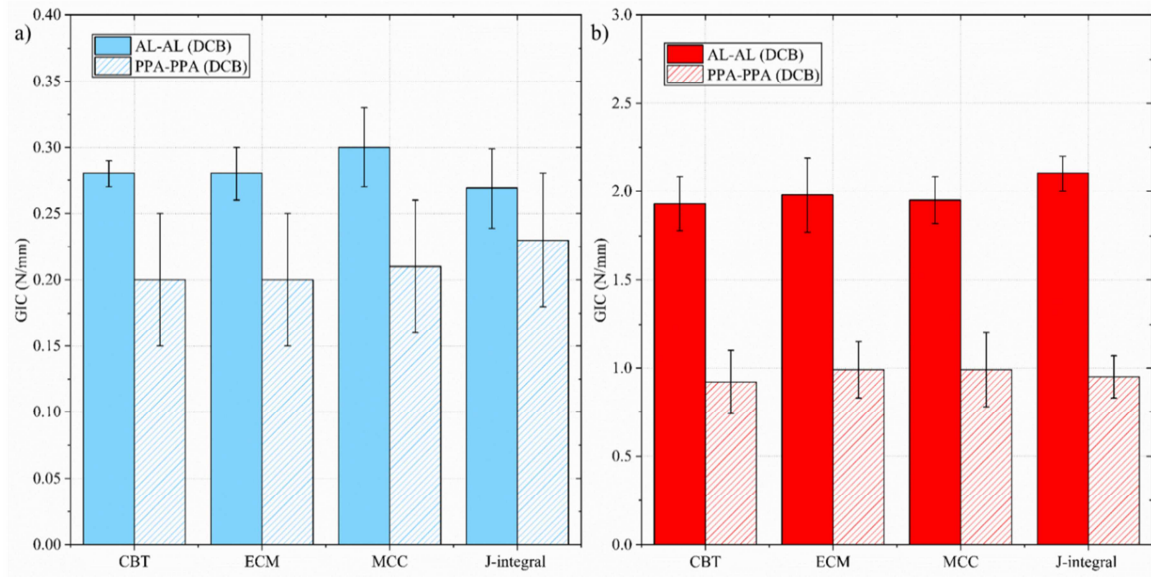


Figure 1: Comparing average fracture energy calculated with different methods for AL-AL and PPA-PPA DCB specimens with (a) epoxy-based and (b) polyurethane adhesives